Presented at SPIE Defense and Security Symposium, Orlando, FL 2004

A One-Dimensional Approach for Iris Identification

Yingzi Du[a*], Robert Ives[a], Delores Etter[a], Thad Welch[a], Chein-I Chang[b]
[a]Electrical Engineering Department, United States Naval Academy, Annapolis, MD 21402;
[b]Dept. of Computer Science and Electrical Engineering, Univ. of Maryland, Baltimore County, Baltimore, MD 21228

ABSTRACT

A novel approach to iris recognition is proposed in this paper. It differs from traditional iris recognition systems in that it generates a one-dimensional iris signature that is translation, rotation, illumination and scale invariant. The *Du* Measurement was used as a matching mechanism, and **t**his approach generates the most probable matches instead of only the best match. The merit of this method is that it allows users to enroll with or to identify poor quality iris images that would be rejected by other methods. In this way, the users could potentially identify an iris image by another level of analysis. Another merit of this approach is that this method could potentially improve iris identification efficiency. In our approach, the system only needs to store a one-dimensional signal, and in the matching process, no circular rotation is needed. This means that the matching speed could be much faster.

Keywords: Iris Identification, *Du* Measurement, one-dimensional iris signature.

1. INTRODUCTION

Biometrics uses unique and measurable physical, biological, or behavioral characteristics to establish identification, and to perform identity verification or automated recognition of a person [1-5]. The three tasks of biometrics [1-2] are:

- Verification: "Are you who you say you are?"
- Identification: "You are in my database, can I find you?"
- Watchlist: "Are you in my database? If so, who are you?"

"Watchlist" refers to the act of scrutinizing individuals to determine if they belong to a selected group, such as criminals. Within these three tasks, identification (one-to-few match) is more difficult than verification (one-to-one match), while watchlist (one-to-many) would be the most difficult.

The iris is a protected internal organ whose random texture is stable throughout life [1-2]. Compared with other biometric features such as face and fingerprint, iris patterns are more stable and reliable [1-2]. Iris recognition systems are non-invasive to their users [1-11], but require a cooperative subject. For this reason, iris recognition is usually used for verification or identification purpose, rather than for watchlist.

The key step in many current iris pattern recognition algorithms is to transfer the iris pattern into a two-dimensional code [6-9]. To eliminate the effect of eye tilt, circular rotation of the iris pattern is usually necessary in iris matching and identification algorithms [6-7,9-10]. Among them, Daugman's 2-D Gabor wavelet approach has been successfully tested using a large-scale iris database and has been commercialized by Iridian [11].

In this paper, we propose a novel approach for iris identification. We develop gray scale invariant Local Texture Patterns (LTP) to generate a one-dimensional signature for each iris image, and use an Information Divergence-Based Du measurement developed by Du *et al* [12] to measure the similarity between the test iris signature and those signatures in the database. In contrast to traditional iris recognition methods [6-10], we compare the input iris image to all iris patterns in the database and list them according to similarity. As a result, we generate the top ten closest matches. This method could potentially improve the iris identification computational efficiency, since the system only needs to store a one-dimensional signal, and in the matching process, no circular rotation is needed.

Portions of this research use the iris image database collected by the Institute of Automation, Chinese Academy of Sciences (CASIA) [20]. The organization of this paper is as follows: Section 2 introduces the *Du* measurement; Section 3 develops the gray scale invariant LTP; Section 4 discusses the system architecture; Section 5 shows the experimental results; and Section 6 draws conclusions.

*yingzidu@ieee.org; phone: 1 410 293-6158; fax 1 410 293-3493

2. THE *DU* MEASURE

The Spectral Angle Mapper (SAM) [12,13,14] has been widely used as a spectral similarity measure for multi/hyper-spectral signals [12-14]. The SAM measures the angle between the spectral vectors $\mathbf{r} = (r_1, r_2, \cdots, r_L)^T$ and $\mathbf{s} = (s_1, s_2, \cdots, s_L)^T$ and is given by:

$$\mathrm{SAM}(\mathbf{r},\mathbf{s}) = \cos^{-1}\left(\frac{\langle \mathbf{r},\mathbf{s}\rangle}{\| \mathbf{r} \| \times \| \mathbf{s} \|}\right). \tag{1}$$

Here, $\langle \mathbf{r},\mathbf{s}\rangle$ is the inner product of vectors $\mathbf{r}$ and $\mathbf{s}$, $\langle \mathbf{r},\mathbf{s}\rangle = \sum_{l=1}^{L} r_l s_l$, $\| * \|$ is the vector norm (2-norm), and $\| \mathbf{r} \| = \sqrt{\langle \mathbf{r},\mathbf{r}\rangle}$ and $\| \mathbf{s} \| = \sqrt{\langle \mathbf{s},\mathbf{s}\rangle}$.

Let $\mathbf{p} = (p_1, p_2, \cdots, p_L)^T$ and $\mathbf{q} = (q_1, q_2, \cdots, q_L)^T$ be the two probability mass functions generated by vectors **r** and **s**. The Spectral Information Divergence (SID) [12,14] between vectors **r** and **s** is defined as:

$$\mathrm{SID}(\mathbf{r},\mathbf{s}) = D(\mathbf{p} \| \mathbf{q}) + D(\mathbf{q} \| \mathbf{p}). \tag{2}$$

Here $D(\mathbf{p} \| \mathbf{q})$ is the relative entropy (also known as Kullback-Leibler information measure) [12,14] of **q** with respect to **p**, where $D(\mathbf{p} \| \mathbf{q}) = \sum_{j=1}^{L} p_j \log(p_j / q_j)$. Also, $D(\mathbf{q} \| \mathbf{p})$ is the relative entropy of **p** with respect to **q**, where $D(\mathbf{q} \| \mathbf{p}) = \sum_{j=1}^{L} q_j \log(q_j / p_j)$. Note that $D(\mathbf{p} \| \mathbf{q})$ is usually different from $D(\mathbf{q} \| \mathbf{p})$.

Recently, Du *et al* [12] developed the *Du* measure, also known as (SID,SAM)-mixed measure. It is defined as:

$$\mathrm{Du}(\mathrm{r},\mathrm{s}) = \mathrm{SID}(\mathbf{s},\mathbf{s}') \times \tan(\mathrm{SAM}(\mathbf{s},\mathbf{s}')). \tag{3}$$

The *Du* measure has been shown to take advantage of the strengths of both SID and SAM [12], and is used in Section 4 as a key to measure the similarity between two iris signatures.

3. GRAY SCALE INVARIANT LOCAL TEXTURE PATTERNS (LTP)

Analyzing iris patterns is a key step for iris pattern recognition and verification. A major problem in analyzing iris patterns (iris textures) is that they are often not uniform due to variations in orientation, scale, contrast, or illumination. The problem of orientation variations will be solved by generating a one-dimensional signature and is described in detail in Section 4. The problem of scale variations will be solved by the Mask Generation Module described in Section 4.2. The problem of contrast variations will be solved by using the *Du* measure described in Section 2 and the details of the application of the *Du* measure for iris identification are described in Section 4. To solve the problem of illumination (gray scale) variations, we designed the gray scale invariant Local Texture Patterns (LTP). This is a very simple method that could be applied to non-iris gray scale imagery for texture analysis as well.

Let T be a set of pixels in an X-by-Y window and let B be the center subset of x-by-y pixels in window T, where X > x and Y>y (Fig. 1). We subtract the mean of the gray value of the window T from the gray values of the pixels in the

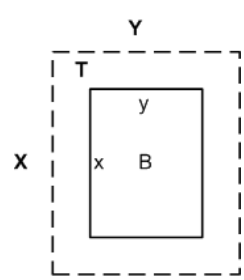

Figure 1. Window T and Window B used in calculating the LTP.

window B to form the LTP for the pixels of set B. The LTP of a pixel at coordinate (i,j) inside window B is given as:

$$LTP_{ij} = I_{ij} - m_T \ , \ I_{ij} \in B \tag{4}$$

where I_{ij} is the gray scale value of the pixel (i,j) in B, and m_T is the mean gray scale value inside window T. The reason for selecting window T to be slightly larger than window B is so that the local mean m_T be can be a better approximation to the true mean value and is less affected by noise. In addition, by computing LTPs using an overlapping T window, boundary discontinuities are avoided. Examples of the overlapping windows are given in Fig. 2.

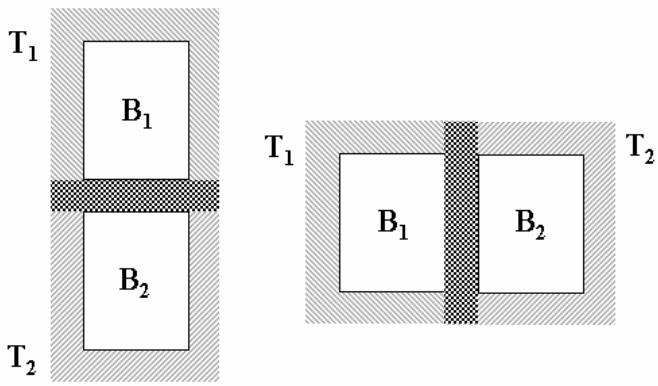

(a) (b)

Figure 2. Overlapping T windows.

4. IRIS RECOGNITION SYSTEM ARCHITECTURE

The proposed system is comprised of the following modules: Preprocessing, Mask Generation, LTP, Iris Signature Generation, Enrollment, Iris Identification, and Iris Signature Database. The system architecture is depicted in Fig. 3, and is described in the following.

4.1. Preprocessing Module

The Preprocessing Module locates the various components of the iris boundary. In particular, we find the limbic (outer) boundary of the iris, the pupillary (inner) boundary of the iris, and the eyelids. As the first step, we discard every other row and column of the original iris image to reduce it (Fig. 4(a)) to ¼ of the original size to speed up the processing (Fig. 4(b)). The Canny method [15] was applied to this image for edge detection. The edge image was then

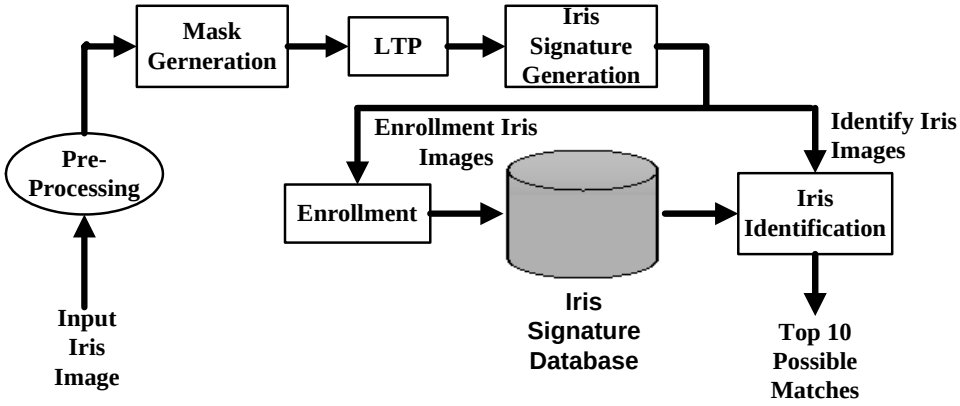

Figure 3. Iris Identification System Architecture

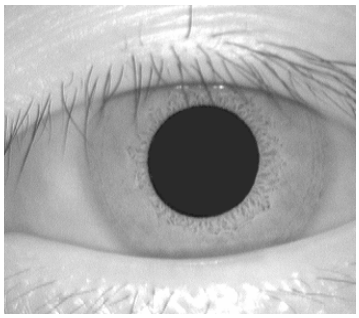

(a) Original iris image (002_1_1 in CASIA database)

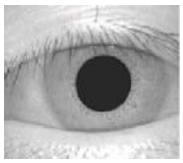

(b) ¼ size iris image

(c) Edge of the iris image

Figure 4. Edge Detection of Iris image

thresholded and is shown in Fig. 4(c). There is a clear circle in the edge image in Fig. 4(c) that represents the outer edge of the pupil. The edges above and below the circle are the edges of eyelids and eyelashes. The circle parameters (center (x_0, y_0) and radius r_0) are then estimated and optimized for the pupillary boundary.

The entire image is then transformed to polar coordinates with center (x_0, y_0). On the polar axis, the limbic boundary is very nearly horizontal. A horizontal Sobel filter [7,16,17,18] is applied to detect the horizontal edges. The longest horizontal edge after the pupillary boundary is the limbic boundary. Fig. 5(a) shows the iris image in polar coordinates. Fig. 5(b) shows the iris image in Fig. 4(a) after the inner and outer boundaries have been detected.

To remove the effects of eyelashes or high reflectance pixels (glare), a determination is made if any pixel value in the image is an outlier. To do this, the variances of the gray scale intensities are computed in a 3-by-3 window about each location. If the computed variance is above a selected threshold, the pixel at that location can be reasonably

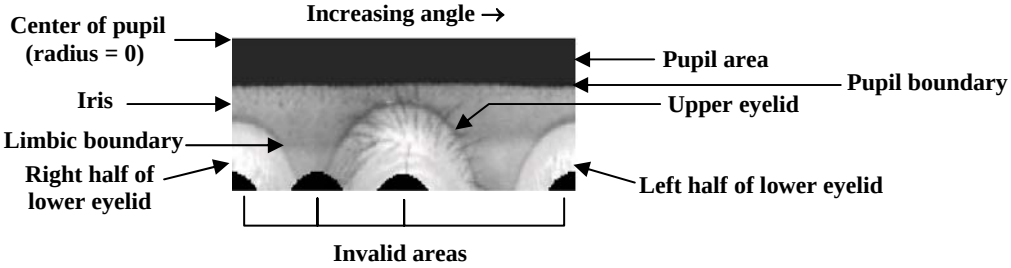

(a) The iris image from Fig. 4(a) in polar coordinates.

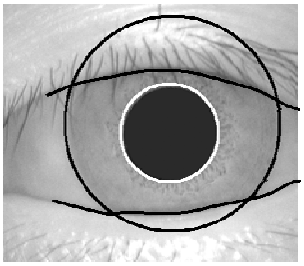

(b) The iris image from Fig. 4(a) after boundary detection.

Figure 5. Iris Boundary Detection.

discarded.

4.2. Mask Generation Module

The size of the same iris taken at different times may be variable in the image as a result of changes in the camera-to-face distance [7]. Due to stimulation by light or for other reasons the pupil may be constricted or dilated. These factors will change the iris resolution, and the actual distance between the pupillary and the limbic boundary.

To solve these problems, the iris image is processed [7,9] to ensure the accurate location of the virtual circle and to fix the resolution. We normalize this distance to be a constant $\tilde{L}$ pixels for all iris images. The value of $\tilde{L}$ should be decided based on the overall resolution of the iris images in the database. In our experiments, the iris images are all 280-by-320 pixels. The distance from the pupil to the limbic usually fell in the range of 55~70 pixels. In this case, $\tilde{L}$ should be some value between 50 and 60, because it would be easier to shrink the image size via averaging pixel values than to enlarge the image via interpolating the pixels (which may introduce false patterns). In our case, we select $\tilde{L}$ =56.

The iris area is transformed to the resolution invariant polar coordinates (which are different from the standard polar coordinates used in Section 4.1) [7]. For each pixel in the original iris image located at rectangular coordinates (x_i,y_i), we compute its polar coordinates (r_i,θ_i) as:

$$r_i = \frac{\tilde{L}}{L}\left(\sqrt{(x_i - x_0)^2 + (y_i - y_0)^2} - r_0\right), \qquad \theta_i = \begin{cases} \arcsin\left(\dfrac{y_i - y_0}{x_i - x_0}\right) & y_i \geq y_0 \\ \pi + \arcsin\left(\dfrac{y_i - y_0}{x_i - x_0}\right) & y_i < y_0 \end{cases}. \tag{5}$$

At the same time, the boundary positions are transferred to the resolution invariant polar coordinates. Fig. 6(a) shows the generated iris mask, where white represents the locations of iris pattern areas, and black represents the non-iris pattern areas, such as pupil pixels, eyelids, and eyelashes. Fig. 6(b) shows the resulting iris patterns after applying the mask. Note that the mask is resolution (scale) invariant.

4.3. LTP Module

After applying the mask to the iris pattern in the invariant resolution polar coordinates (Fig. 6(b)), the LTP Module generates the local iris patterns using Eq. (4). We set the size of window T to be 15-by-7 and window B to be 9-by-3. Note that the left-most column of the image in Fig. 6(b) is connected to the right-most column, so there are no actual left or right edges that would introduce artifacts. To reduce the effect of non-iris pixels (they appear black in Fig. 6(b)), if more than 50% of pixels in window B or more than 60% of pixels in window T are non-iris patterns, we discard them as non-iris pattern areas.

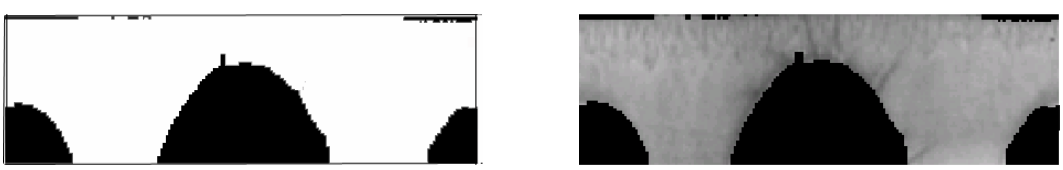

(a) The resolution invariant mask (b) The resolution invariant iris patterns

Figure 6. Iris Mask and Iris Patterns.

4.4. Iris Signature Generation Module

After local iris patterns were calculated by the LTP Module, the Iris Signature Generation Module will build a one-dimensional signature for each iris image by averaging the LTP values of each row. If more than 60% of the pixels in a row are non-iris, we set the signature value for that row to be –1. Since the iris-patterns in the top and bottom three rows are usually very noisy, we removed these six rows when building the iris pattern. Fig. 7 shows the one-dimensional signature for the iris image in Fig. 4(a).

In Fig. 4(a), observe that the iris pixels near the pupillary area have more variation than iris pixels farther from the pupil. In Fig. 7, this feature is characterized by relatively high values of LTP along the left side of the plot (representing areas closer to the pupil): these values are the average LTP values of each row in the resolution invariant polar images.

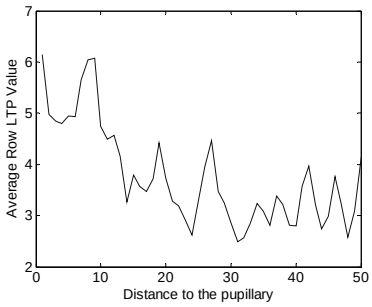

Figure 7. The one-dimensional signature for the iris image in Fig. 4(a).

4.5. Enrollment Module

For an iris pattern to be recognizable in the system, we first need to enroll the iris pattern in the database. Enrollment usually takes multiple iris images of the same iris to register and generate the enrollment iris patterns. In commercial iris recognition systems, such as Panasonic Authenticam [19], iris enrollment requires several (4 for the Authenticam) high quality iris images. Here, our system only uses 3 iris images. In the CASIA iris database, each iris has 7 images. We take the first 3 as enrollment images, compute the three iris signatures for each iris pattern, and average them to get its enrollment iris signature (Fig. 8).

Since the iris signatures are not directly related to the angles of the iris patterns, eye restoration would not affect the one-dimensional signal. In this way, we invented a rotation invariant iris signature.

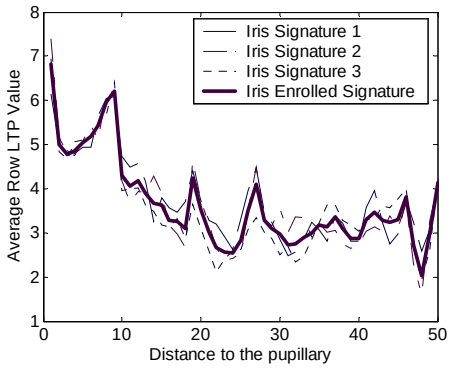

Figure 8. The iris signatures and their enrolled signature. Iris Signature 1, 2, and 3 are from iris images 002_1_1, 002_1_2, and 002_1_3 in the CASIA database.

4.6. Iris Signature Database

Enrolled iris signatures were stored in the Iris Signature Database. The CASIA database contains imagery for a total of 108 different irises. We enrolled all of these 108 irises (overall, using 324 iris images for enrollment) and stored them in the database.

4.7. Iris Identification Module

When an iris image is presented for identification, its iris signature is generated by the Iris Signature Generation Module, and we attempt to match it with the enrolled iris signatures inside the database. The matching score is based on the *Du* measurement [12] introduced in Section 2. The output of this module is the 10 closest matches from the database.

5. EXPERIMENTAL RESULTS

In commercial iris recognition systems, the system will automatically reject unclear iris images and requires the eye to be open wide, using video technology to select the best iris images for enrollment. Images such as those shown in Fig. 9(a-c) may not be acceptable. Because we are using the CASIA database, we cannot control the quality of the images. However, our system would use the images in Fig. 9(a-c) anyway. The resulting iris signature is shown in Fig. 9(d).

In Fig. 9(a)-(c), the quality of the three enrollment iris images is poor. The upper eyelids and eyelashes have hidden the upper half and a portion of the lower half iris patterns. In Fig. 9(a) and (c), the reflectance of the lower eyelids has an illumination effect on nearby iris patterns. As a result, the iris patterns in the outer circle have been hidden largely by the eyelids, eyelashes or affected by the abnormal illumination. In Fig. 9(d), for iris signature 2 and 3, the LTP is –1 when the distance to pupil is larger than 42. This is reasonable because we cannot get 40% or more valid iris patterns in these iris circles. Because of this, the resulting signature will be same as that of iris signature 1 in these areas. Also, we found large variances in the iris signature near the pupillary areas (distance less than 3), especially for iris signature 1. In Fig. 9(a), we notice that the eye is more closed than in the other images. This means that more iris patterns in this area have been hidden by eyelashes or eyelids. If we enlarge the iris image (Fig. 10) and look closely, we see there are some smoother iris pattern areas (inside the white elliptic areas) that have been hidden or affected by nearby eyelashes. For this reason, those areas are discarded when generating the iris signature for Fig. 9(a), which results in a higher Average Row LTP values for Fig. 9(a) near the pupillary areas. Overall, the iris images are very similar to each other.

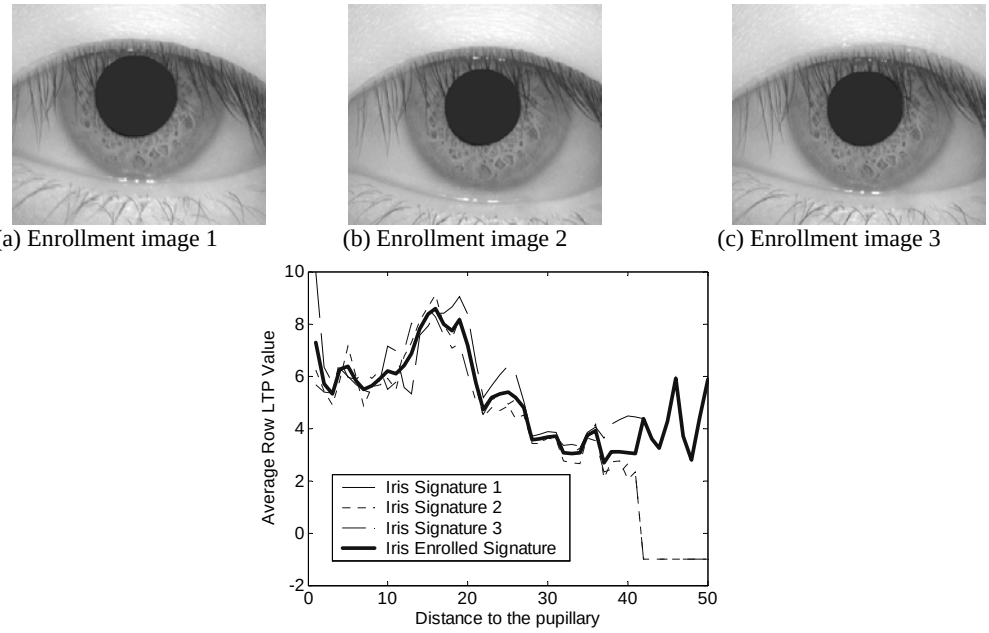

Figure 9. An example of poor enrollment images and their iris signatures. (Enrollment Images 1, 2, and 3 are Iris images 004_1_1, 004_1_2, and 004_1_3 in CASIA database.

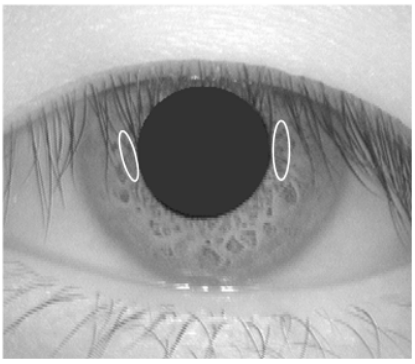

Figure 10. Analysis of Fig. 9(a)

Fig. 11 demonstrates that each iris pattern has its own iris signature. Eight signatures are presented along with one of the irises used to calculate it. Comparing the images of the eight irises, the distinct features of individual irises are apparent.

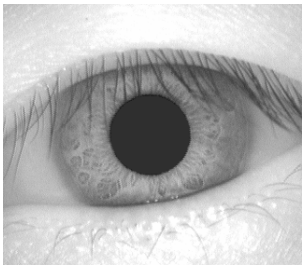

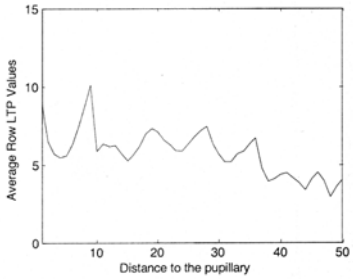

Iris Pattern 1 (Generated from iris images 007_1_1, 007_1_2, and 007_1_3)

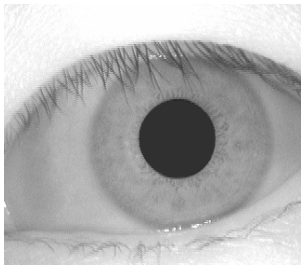

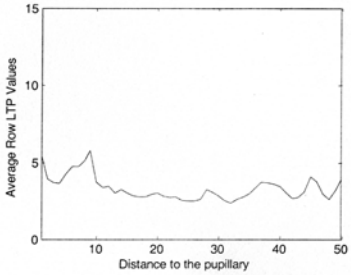

Iris Pattern 2 (Generated from iris images 009_1_1, 009_1_2, and 009_1_3)

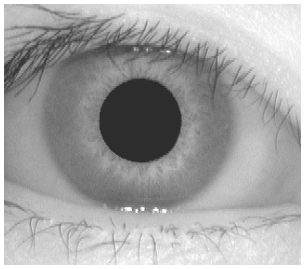

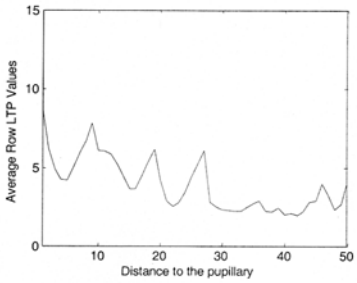

Iris Pattern 3 (Generated from iris images 012_1_1, 012_1_2, and 012_1_3)

Figure 11. Iris images and their iris signatures.

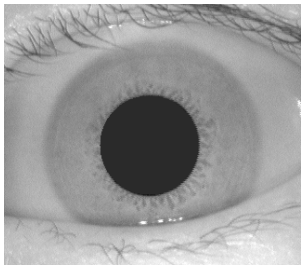
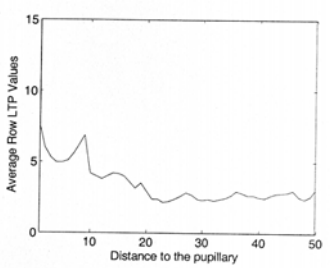

Iris Pattern 4 (Generated from iris images 013_1_1, 013_1_2, and 013_1_3)

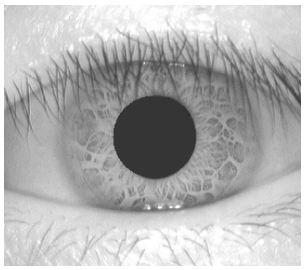
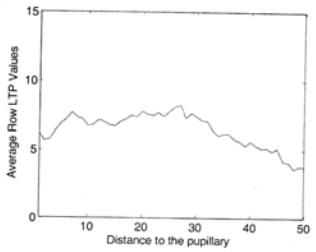

Iris Pattern 5 (Generated from iris images 019_1_1, 019_1_2, and 019_1_3)

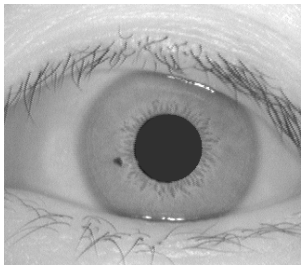
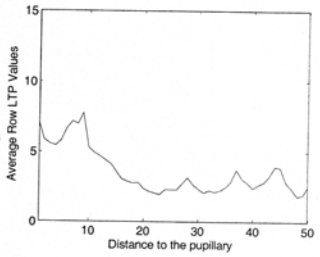

Iris Pattern 6 (Generated from iris images 032_1_1, 032_1_2, and 032_1_3)

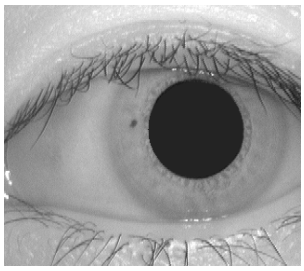
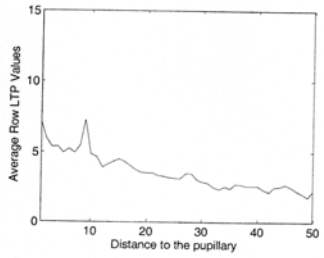

Iris Pattern 7 (Generated from iris images 033_1_1, 033_1_2, and 033_1_3)

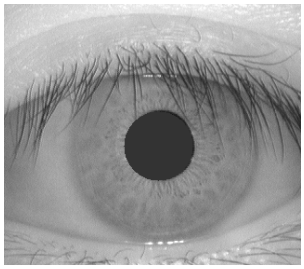
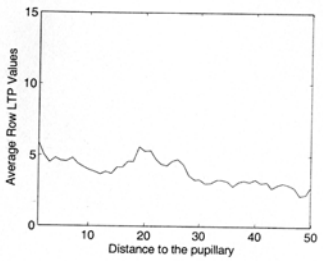

Iris Pattern 8 (Generated from iris images 060_1_1, 060_1_2, and 060_1_3)

Figure 11 (continued). Iris images and their iris signatures

Overall this database contains images of 108 different iris patterns. There are seven iris images for each iris pattern. We used the first three iris images of each pattern to enroll and generate enrollment iris signatures, and 356 iris images to test the algorithm. Using match ranking 1-10 as a measure, all of the tested irises correctly fell into the top 10 ranking. Of these, over 97% fell into the top 5 ranking. The lowest rank was 8; the average rank was 1.6.

6. CONCLUSIONS

A novel approach to iris identification is proposed. It differs from current approaches to iris recognition in several ways. It generates a one-dimensional iris signature that is translation, rotation, illumination and scale invariant. In general, iris recognition could achieve the highest recognition rate among biometrics technologies. However, a weak point of iris recognition is that it needs the users' full cooperation. The merit of our method is that it allows users to enroll poor quality iris images that would be rejected by other methods. In addition, this approach generates a list of possible matches instead of only the best match. In this way, the users could potentially identify the iris image by another level of analysis (such as using traditional iris recognition algorithm for more accurate iris identification). Another merit of our method is that it would allow the iris recognition system to be more tolerable of noise (such as glare introduced by contact lenses or eye glasses). Another merit of this approach is that this method could potentially improve iris identification process computational efficiency. In our approach, the system only needs to store a one-dimensional signal vice a two-dimensional image. Also, in the match processing, no circular rotation is needed, so that matching could be much faster. This work has been filed for patent.

ACKNOWLEDGEMENTS

The authors wish to thank the National Laboratory of Pattern Recognition Institute of Automation at Chinese Academy of Sciences, for providing the database used for these experiments.

REFERENCES

[1] D.M. Etter, "Biometrics: The Promises and the Challenges", presentation at the Biometric Consortium Conference, VA, U.S.A., 2003.http://www.biometrics.org/bc2003/program.htm

[2] Woodward, N.M. Orlans, and P.T. Higgins, *Biometrics*, The McGraw-Hill Company, Berkeley, California, 2002.

[3] Y. Du, R. W. Ives, D. M. Etter, and T.B. Welch, "A Multidisciplinary Approach to Biometrics", submitted to IEEE Transaction on Education, (2004).

[4] Y. Du, R. W. Ives, D. M. Etter, and T. B. Welch, "Biometric Signal Processing Laboratory", accepted by IEEE Conference on Acoustics, Speech and Signal Processing (ICASSP), 2004.

[5] R. W. Ives, D. M. Etter, Y. Du, and T. B. Welch, "Development of an Undergraduate Course in Biometric Signal Processing ", accepted by the American Society for Engineering Education Annual Conference & Exposition (2004).

[6] J. Daugman, "High Confidence Visual Recognition of Persons by a Test of Statistical Independence", Pattern Analysis and Machine Intelligence, IEEE Transaction on, Vol. 15, No. 11, pp. 1148-1161, 1993.

[7] Y. Du, R. W. Ives, D. M. Etter, T.B. Welch, and C.I-Chang, "A New Approach to Iris Pattern Recognition for Biometric Identification", submitted to *IEEE International Conference on Pattern Recognition* (ICPR), (2004).

[8] R.P. Wildes, J.C. Asmuth, G.L. Green, S.C. Hsu, R.J. Kolczynski, J.R. Matey, and S.E. McBride, "A Machine Vision System for Iris Recognition", Mach. Vision Application, Vol. 9, pp.1-8, 1996.

[9] W.W. Boles and B. Boashash, "A Human Identification Technique Using Images of the Iris and Wavelet Transform", *IEEE Transactions on Signal Processing*, Vol. 46, No. 4, pp. 1185-1188, 1998.

[10] Y. Zhu, T. Tan, and Y. Wang, "Biometric Personal Identification Based on Iris Patterns", *15th International Conference on Pattern Recognition*, Vol. 2 , pp. 801 –804, 2000.

[11] J.E. Siedlarz, "Iris: More detailed than a fingerprint", *IEEE Spectrum*, vol. 31, pp. 27, 1994.

[12] Y. Du, C.-I. Chang, H. Ren, F.M. D'Amico, J. Jensen, J., "A New Hyperspectral Discrimination Measure for Spectral Similarity", *Optical Engineering*, Vol. 43, No. 8, 2004.

[13] R.A. Schowengerdt, *Remote Sensing: Models and Methods for Image Processing*, 2nd Ed., Academic Press (1997).

[14] C.-I Chang, "An information theoretic-based approach to spectral variability, similarity and discriminability for hyperspectral image analysis", *IEEE Trans. on Information Theory*, 46(5), pp. 1927-1932 (2000).

[15] J. Canny, "A Computational Approach to Edge Detection", *IEEE Transactions on Pattern Analysis and Machine Intelligence*, Vol. 8, No. 6, Nov 1986.

[16] R.C. Gonzales and R.E. Woods, *Digital Image Processing*, Second Edition, Prentice Hall, Upper Saddle River, New Jersey, 2001.
[17] Y. Du, C.-I. Chang, and P.D. Thouin, "An Automated System for Text Detection in Individual Video Images", *Journal of Electronic Imaging*, Vol. 12, No. 3, pp. 410-422, (2003).
[18] Y. Du, *Text Detection and Restoration of Color Video Images*, Ph.D. Dissertation, University of Maryland, Baltimore County, 2003.
[19] http://www.iridiantech.com/, (2004).
[20] CASIA Iris Image Database, http://www.sinobiometrics.com